# Stitched α-Helical Peptides via Bis Ring-Closing Metathesis

Gerard J. Hilinski,[†,∇] Young-Woo Kim,[†,∥,∇] Jooyeon Hong,[‡] Peter S. Kutchukian,[†,#] Charisse M. Crenshaw,[†,○] Shaunna S. Berkovitch,[†,⊥] Andrew Chang,[†,◆] Sihyun Ham,*,[‡] and Gregory L. Verdine*,[†]

[†]Department of Chemistry and Chemical Biology and Department of Stem Cell and Regenerative Biology, Harvard University, Cambridge, Massachusetts 02138, United States

[‡]Department of Chemistry, Sookmyung Women's University, Hyochangwon-gil 52, Yongsan-ku, Seoul 140-742, Korea

**S** *Supporting Information*

**ABSTRACT:** Conformationally stabilized α-helical peptides are capable of inhibiting disease-relevant intracellular or extracellular protein−protein interactions *in vivo*. We have previously reported that the employment of ring-closing metathesis to introduce a single all-hydrocarbon staple along one face of an α-helical peptide greatly increases α-helical content, binding affinity to a target protein, cell penetration through active transport, and resistance to proteolytic degradation. In an effort to improve upon this technology for stabilizing a peptide in a bioactive α-helical conformation, we report the discovery of an efficient and selective bis ring-closing metathesis reaction leading to peptides bearing multiple contiguous staples connected by a central spiro ring junction. Circular dichroism spectroscopy, NMR, and computational analyses have been used to investigate the conformation of these "stitched" peptides, which are shown to exhibit remarkable thermal stabilities. Likewise, trypsin proteolysis assays confirm the achievement of a structural rigidity unmatched by peptides bearing a single staple. Furthermore, fluorescence-activated cell sorting (FACS) and confocal microscopy assays demonstrate that stitched peptides display superior cell penetrating ability compared to their stapled counterparts, suggesting that this technology may be useful not only in the context of enhancing the drug-like properties of α-helical peptides but also in producing potent agents for the intracellular delivery of proteins and oligonucleotides.
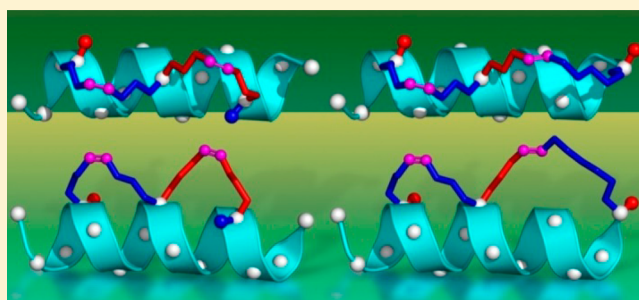
## INTRODUCTION

Intracellular protein−protein interactions serve pivotal roles in nearly all aspects of cell function, and their involvement in disease pathophysiology is well-established. Therapeutic intervention at these critical interfaces has proven frustrating, however, because the relatively flat contact surfaces participating in protein−protein interactions are devoid of hydrophobic pockets and therefore poorly suited for targeting by small molecules.[1] Though extracellular protein−protein interactions are amenable to interference with biologics such as monoclonal antibodies, these large molecules are incapable of penetrating the cell membrane and accessing the cytoplasm and nucleus. Thus, there is significant interest in the development of alternative types of molecules that feature the cell penetrating ability of small molecules yet can engage protein surfaces with the efficacy of biologics. Toward this end, we and others have pursued an approach that involves deconstructing proteins down to "dominant interfering" peptides comprising a minimal protein-targeting surface and then stabilizing the bioactive conformation through the introduction of a synthetic cross-link. Though numerous synthetic buttressing systems have been reported to stabilize a variety of folded peptide conformations, the ubiquity of α-helices in protein−protein interfaces[2−4] has led to an intense focus on this particular secondary structure. The α-helical conformation has been stabilized using many different types of cross-links, including lactam,[5−8] disulfide,[9−11] thioether,[12] azobenzene,[13] hydrazone,[14] triazole,[15] biphenyl,[16] bis-triazoylyl,[17] oxime,[18,19] perfluoroaryl,[20] and carbamate.[21]

Ruthenium-catalyzed ring-closing metathesis (RCM) has proven useful as a means of introducing helix-constraining cross-links into peptides, including 3_{10}-helices by Grubbs and co-workers[22−24] and α-helices by Arora and co-workers.[25] We have previously reported one such metathesis-enabled α-helix reinforcement system, the all-hydrocarbon staple, which unlike all previous systems incorporates both α-methyl groups and a macrocyclic all-hydrocarbon ring as two distinct helix-stabilizing elements (Figure 1).[26−29] This system affords exceptionally high levels of α-helix induction and nucleation, and as a direct result can increase target binding affinity, serum stability, and *in vivo* half-life.[30−32] Perhaps most significantly, however, it has been shown in multiple studies employing different stapled peptides that the presence of the hydrocarbon staple causes these peptides to be actively transported into mammalian cells
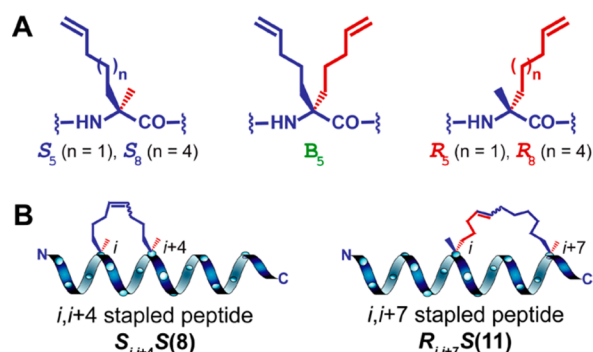
**Figure 1.** (A) Olefin-bearing amino acids used in this study. (B) Schematic structures of helical peptides constrained by an all-hydrocarbon staple across one turn ($i, i + 4$) or two turns ($i, i + 7$) of an $\alpha$-helix. The nomenclature $S_{i,i+4}S(8)$ refers to an 8-carbon metathesized cross-link with ($S$)-configuration at positions $i$ and $i + 4$; $R_{i,i+7}S(11)$, an 11-carbon cross-link with ($R$)- and ($S$)-configuration at positions $i$ and $i + 7$, respectively.

through endocytic vesicle trafficking.[33−36] Moreover, these molecules can efficiently escape endosomes and access both cytoplasmic and nuclear targets, as they are well below the 40 kDa exclusion size of the nuclear pore complex. The therapeutic potential of stapled peptides has been underscored by studies demonstrating efficacy in animal models of disease,[33,37−41] and Aileron Therapeutics has initiated clinical trials of the first stapled peptide therapeutics.

The first-reported all-hydrocarbon staples were incorporated into a peptide through the introduction of two $\alpha$-methyl,$\alpha$-alkenylglycine units at positions separated by either three ($i, i + 4$; one helical turn) or six ($i, i + 7$; two helical turns) intervening residues. The macrocyclic ring was then closed via ruthenium-catalyzed RCM to form the $S_{i,i+4}S(8)$ and $R_{i,i+7}S(11)$ staple, respectively, with the nomenclature specifying the configurations of the stapling residues and the final length of the cross-link (Figure 1B). Recently, we have reported a hydrocarbon staple that involves the introduction of two $\alpha$-methyl, $\alpha$-alkenylglycine units at positions separated by two intervening residues ($i, i + 3$ one helical turn) and subsequent closure via ruthenium-catalyzed RCM to form the $R_{i,i+3}S(8)$ staple.[28] These stapling systems have now been employed successfully by our laboratory and others against a wide variety of high-value biological targets, as reviewed recently by Walensky and Bird.[32]

All-hydrocarbon staples can serve as powerful nucleators of $\alpha$-helical structure, such that the incorporation of a single staple into a 4, 5, or 8 amino acid stretch of a peptide can induce helical structure throughout a much longer sequence. Additionally, two or more separate and distinct staples can be incorporated into a single peptide, conferring increased proteolytic resistance and enhanced biological activity.[37,41] Unsurprisingly, however, the nucleated stretches of stapled peptides do not show the same extent of protease resistance as the stapled portion. We therefore sought to extend the synthetically constrained region over a larger stretch of the peptide, with the aim of conferring protease resistance even in harsh environments such as those encountered in the human intestinal tract.

Here we report a next-generation version of the hydrocarbon-stapling system in which dual hydrocarbon staples emerge from common attachment points in the peptide, thereby creating spiro macrocyclic ring junctions, a type of ring fusion known to be exceptionally rigidifying. To our knowledge, this is the first report of $\alpha$-helical peptides stabilized by multiple connected staples. We envision this system of installing contiguous staples along one face of the $\alpha$-helix as akin to peptide "stitching". In this article, we describe highly regio- and stereospecific RCM reactions on an $\alpha$-helical scaffold, leading to efficient, clean formation of stitched $\alpha$-helical peptides. We also demonstrate that peptide stitching provides superior helix induction, thermal stability, proteolytic resistance, and cell permeability relative to peptide stapling.

## ■ EXPERIMENTAL METHODS

**Peptide Synthesis.** The peptides were prepared using Fmoc chemistry on Rink Amide MBHA resin (NovaBiochem) with a loading capacity of 0.59 mmol/g. The dry resin was swelled with $CH_2Cl_2$ followed by 1-methyl-2-pyrrolidinone (NMP) before use. The Fmoc protecting group was removed by treatment with 25% piperidine in NMP (4 × 5 min). Natural amino acids were coupled for 60 min using (1-cyano-2-ethoxy-2-oxoethylidenaminooxy)dimethylamino-morpholino-carbenium hexafluorophosphate (COMU) as the activating agent (4 equiv), 4 equiv of Fmoc-protected amino acid, and 8 equiv of diisopropyl ethylamine (DIPEA) in NMP. For the coupling of olefin-bearing amino acids, a reaction time of 2 h was used with Fmoc-protected amino acid (3 equiv), COMU (3 equiv), and DIPEA (6 equiv). After each coupling or deprotection reaction, the resin was washed with NMP (5 × 1 min).

**Metathesis and Purification.** Ring-closing metathesis of resin-bound N-Fmoc, side-chain-protected peptides was performed using 20 mol % of Grubbs I catalyst in 1,2-dichloroethane (DCE) for 2 h at room temperature. The reactions were monitored by LC/MS after cleavage of the peptides from a resin aliquot, and additional treatments with fresh catalyst were used to obtain more complete conversion in many cases. After the reaction solution was drained, the resin was washed with DCE (3 × 1 min) and $CH_2Cl_2$ (3 × 1 min). After Fmoc group removal, Fmoc-Ebes-OH (N-Fmoc-2,2′-(ethylenedioxy) bis (ethylamine) monosuccinamide) or Fmoc-$\beta$-alanine-OH was coupled followed by Fmoc group deprotection. For the acetylated analogs, the N-terminal amine was treated with 30 equiv of acetic anhydride and 60 equiv of DIPEA in NMP for 45 min. For the fluoresceinated analogs, the peptide N-termini were exposed overnight to fluorescein isothiocyanate (7 equiv) in DMF in the presence of DIPEA (10 equiv) at room temperature. The resin was washed with DMF (3 × 3 min), $CH_2Cl_2$ (3 × 3 min), and methanol (3 × 3 min) and dried in vacuo overnight. The peptides were deprotected and cleaved from the resin by treatment with a mixture of trifluoroacetic acid/triisopropylsilane/water (95/2.5/2.5) for 2−3 h and precipitated by addition of a 1:1 mixture of n-pentane and diethyl ether. The precipitate was collected by centrifugation, dissolved in a 1:1 mixture of acetonitrile and water, and filtered to remove the resin. The products were purified by reverse-phase HPLC using a Zorbax C18 column (Agilent, 5 $\mu$m, 9.4 × 250 mm) and characterized by liquid chromatography/mass spectrometry (LC/MS) using a Zorbax C18 column (Agilent, 3.5 $\mu$m, 2.1 × 150 mm) and amino acid analysis.

**Circular Dichroism (CD).** Peptides were dissolved in 20 mM potassium phosphate buffer (pH 6.5), and the concentrations were determined by absorbance spectroscopy (extinction coefficient for tryptophan, $\lambda_{280} = 5690$ cm$^{-1}$). CD spectra were collected on a Jasco J-710 spectropolarimeter equipped with a temperature controller using the following standard measurement parameters: 0.5 nm step resolution, 20 nm/s speed, 10 accumulations, 1 s response, 1 nm bandwidth, 0.1 cm path length. All spectra were converted to a uniform scale of molar ellipticity after background subtraction. Curves shown are smoothed with standard parameters. Temperature-dependent CD spectra of each peptide (94−100 $\mu$M) were recorded at varying temperatures (every 10 °C from 10 to 90 °C) from 260 to 185 nm. To generate thermal unfolding curves, the ellipticity at 222 nm was measured every 1 °C from 10 to 90 °C with a temperature slope of 3 °C/min. To obtain the melting temperatures, we analyzed the

thermal unfolding curves using a two-state model with a 95% confidence interval as previously described.[43] Most stitched peptides did not have a cooperative melting transition point in this temperature range, and therefore their melting temperatures were indeterminable by this method.

**Molecular Modeling.** A Monte Carlo conformational search was performed to locate all low-energy conformations of each linker in the helical state. To generate starting conformations for the MC search, a 15-residue polyalanine peptide was built with a right-handed helical conformation using MacroModel's Maestro GUI.[44] Hydrocarbon cross-links were manually added and then fully minimized, while all non-cross-linker atoms were held frozen. For each isomer, at least two distinct 5−10,000 step Monte Carlo conformational searches were run. For all calculations, energies were evaluated using the OPLS2005 force field as implemented in Macromodel. For all minimizations the Polak−Ribiere conjugate gradient (PRCG) method was employed, and the convergence criterion for the minimization of gradient norm was set to <0.05 kJ/mol·Å. We employed the GB/SA solvation treatment,[45] modeling the solvent as chloroform as all metathesis reactions were carried out in 1,2-DCE. Bond dipole cutoffs were employed to truncate the electrostatic and GB terms. Nonbonded cutoffs were as follows: 8 Å in van der Waals, 99999.0 Å in charge−charge (effectively infinite), $20^{3/2}$ Å (89.4 Å) in charge−dipole, and 20 Å in dipole−dipole. Harmonic constraints (100 kJ/mol) were placed on each backbone dihedral angle to maintain the helical conformation throughout the search. At each step of the Monte Carlo search, 2−5 cross-link dihedrals were randomly selected, and their values were adjusted by 0−180°. The C-terminal C−C bond adjacent to each olefin was temporarily broken during each step, allowing for dihedral perturbations along the cross-link, and then reattached after dihedral modification. After each step, up to 500 steps of minimization were performed, if convergence was not achieved in fewer steps, and conformations within 50 kJ of the global minimum were saved. After the search, all remaining structures were fully minimized, and all conformations within 15 kJ of the global minimum were kept, while redundant structures (RMSD < 0.25 Å) were removed. Runs were carried out until the number of new structures obtained after pooling the conformations obtained from the current run with those obtained from all previous runs was <10% of the initial number of structures, suggesting that conformational space had been fully explored (Tables S1 and S2).

**Flow Cytometry.** Jurkat cells (ATCC #TIB-152) were grown in RPMI-1640 supplemented with 10% fetal bovine serum and penicillin/ streptomycin (500 units/mL and 0.5 mg/mL, respectively). For analysis, cells were washed with PBS and resuspended in serum-free RPMI-1640 at a density of $10^6$ cells/mL. Cells were incubated in serum-free media at either 37 or 4 °C for 1 h. Peptides (100 μM in DMSO) were added to 150,000 cells at a final concentration of 1 μM and incubated for 1 h. Samples were resuspended in 500 μL PBS and analyzed by flow cytometry on a LSRII flow cytometer (Becton Dickinson). Experiments were performed independently at least three times. Typically, total Jurkat population size was roughly 1,000. Cells were gated for histogram analysis based on forward and side scatter values indicative of single, live cells: FlowJo's automatic gating tool was used to conservatively isolate the population of single, live cells from the population of cells with low forward and high side scatter. The gated population accounted for 60−80% of the total cell population.

**Confocal Microscopy.** *Temperature-Dependent Cellular Uptake of RNase A Analogs.* U2OS cells (kindly provided by the Schreiber laboratory at the Broad Institute of Harvard and MIT) were cultured in DMEM with 10% fetal bovine serum, seeded at 100,000 cells per chamber in four-chamber slides (Nalge Nunc), and allowed to adhere overnight at 37 °C with 5% CO₂. Thirty minutes prior to peptide addition, slides were either preincubated at 4 °C or left at 37 °C. Cells were washed with PBS and then incubated with 2 μM fluorescein-labeled peptide (originally at 0.1 mM in DMSO) in serum-free DMEM at either 4 or 37 °C for 4 h. After incubation, the cells were washed twice with PBS and then fixed for 15 min in 4% formaldehyde (Sigma-Aldrich) in PBS. Cells were washed twice with PBS, mounted

with Vectashield/DAPI (Vector), and then analyzed using a Zeiss LSM 510 META microscope at 63× and Zeiss LSM image software.

*Cellular Uptake of Oligoarginine Analogs.* HeLa cells were cultured in DMEM with 10% fetal bovine serum, seeded at 20,000 cells per chamber in eight-chamber slides (Nalge Nunc), and allowed to adhere for 48 h at 37 °C with 5% CO₂. Cells were washed with PBS, incubated in serum-free medium at 37 °C for 1 h, and then treated with 5 μM fluorescein-labeled peptide (originally at 1 mM in DMSO) in serum-free DMEM at 37 °C for 4 h. After incubation, the cells were washed twice with PBS and with DMEM without serum and then directly analyzed using a Zeiss LSM 510 META microscope at 25× or 63× and Zeiss LSM image software.

**Peptide Digestion Assay.** 2.5 μL of trypsin solution (5 μM, Sigma) in digestion buffer (0.1 M NH₄HCO₃ buffer, pH 8.0) was added to 250 μL of a fluoresceinated peptide solution (40 μM) in the digestion buffer (enzyme/substrate = 1/800), and the resulting mixture was incubated with rapid shaking (500 rpm) at room temperature. Thirty μL of digestion mixture was taken at 0, 5, 10, 30, 60, 120, minutes and then quenched with 2 μL of trifluoroacetic acid. The residual substrate and hydrolyzed products were quantified by LC/MS-based peak detection at 494 nm. Each experiment was performed in duplicate. The half-life, $t_{1/2}$, was determined by linear regression analysis using KaleidaGraph (Synergy Software) from a plot of ln S (S is % residual substrate) versus time (min) ($t_{1/2} = -\ln 2/$ slope).

## ■ RESULTS AND DISCUSSION

The critical synthetic challenge in producing stitched peptides is to control the regiochemistry and stereochemistry of RCM reactions on peptides having multiple chemically equivalent olefins. Peptide **1**, a typical substrate for stitching, contains four olefins, one each borne on (S)-α-methyl,α-pentenylglycine ($S_5$) and (S)-α-methyl,α-octenylglycine ($S_8$), and two borne on bis-pentenylglycine ($B_5$, 2-(((9H-Fluoren-9-yl)methoxy)-carbonylamino)-2-(pent-4-enyl)hept-6-enoic acid) (Figure 2A). RCM on **1** could therefore in principle generate three possible bis-metathesized products, **2−4** (Figure 2A). Of particular concern was the possibility that the two olefins in $B_5$ might preferentially react with each other during RCM (reaction **a**). To experimentally investigate all the possible RCM reaction pathways shown in Figure 2A, we turned to model studies examining each single-RCM process in isolation (Table 1). Significantly, we found the intraresidue RCM of $B_5$ (reaction **a**) to be highly disfavored, undergoing only 23% conversion to the cyclononenylglycine product with the model peptide under our typical reaction conditions (20 mol % Grubbs I catalyst, 3 × 2h) (Table 1, entry **I**). This RCM reaction was found to be disfavored even with the monomeric Fmoc-protected ethyl ester of $B_5$, in which case the RCM failed completely (Figure S1). These results are in agreement with previous observations that RCM to form a 9-membered carbocyclic ring or larger is typically ineffective.[46,47] Just as undesired reaction **a** proved unfavorable, so also did undesired reaction **b** (entry **II**). Taken together, these results suggested that the **a**+**b** bis-RCM pathway leading to product **2** would be highly unlikely.

To test the likelihood of formation of the undesired product **3**, we tested reaction **c** and found no evidence of product formation (entry **III**). This particular reaction manifold would give an $S_{i,i+4}R(8)$ staple, which is known from both experimental and computational studies to be highly disfavored. In data not shown, the peptide designed to test reaction **d** gave high conversion only after three treatments with catalyst (entry **IV**), whereas the peptide designed to test reaction **f** gave high conversion after only two treatments with catalyst (entry **VI**).
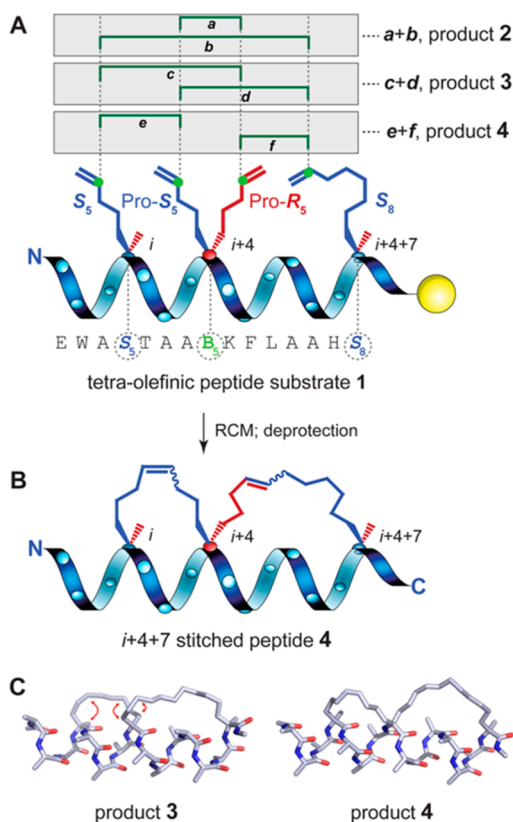
**Figure 2.** (A) The α-helical tetra-olefinic peptide designed to undergo bis-RCM. Three regioisomeric bis-RCM pathways are possible (**a**+**b**, **c**+**d**, and **e**+**f**); these would yield products **2**, **3**, and **4**, respectively. (B) Schematic structure of the main product, the stitched peptide **4**. The stereochemical configuration of the spiro carbon (red dot) was established by modeling. (C) Molecular models of the global minima of all-Ala *i* + 4 + 7 stitched conformers. Product **3** is less stable than product **4** by ~15 kcal/mol due in part to the three syn-pentane interactions highlighted by red arrows.

This result suggests a kinetic preference to form the staple provided by reaction **f**, the product of which, $R_{i,i+7}S(11)$, is also predicted by modeling studies to be thermodynamically more stable than $S_{i,i+7}S(11)$ by 6.5 kcal/mol. Taken together, these results indicate that the **c**+**d** bis-RCM pathway leading to undesired product **3** is unfavorable. By contrast, reactions **e** and **f**, that lead respectively to the well-established $S_{i,i+4}S(8)$ and $R_{i,i+7}S(11)$ staples, proceeded efficiently to provide high conversions to the corresponding stapled products (entries **V** and **VI**).

Overall, these single-stapling studies demonstrated a high degree of regio- and stereochemical control over the RCM reactions on these peptide substrates; the exquisite selectivity of RCM in these peptides is clearly evident from comparison of entries **III** and **V** in Table 1, in which inversion of a single stereogenic center causes a nearly quantitative reaction to fail. We believe that the exceptional selectivity of these reactions with chemically equivalent olefins results from the fact that the peptide substrates are highly helical when undergoing RCM, owing to the presence of multiple helix-promoting α,α-disubstituted residues,[48] the hydrophobic environment of the cross-linking reaction provided by the nonpolar solvent 1,2-DCE,[49] and the protected side-chains.[50] Stated otherwise, the reactions are controlled by α-helix templating.

Of the six possible mono-RCM reactions, the two most efficient ones were **e** and **f**. Should this preferential reactivity be retained in a peptide containing the four olefinic tethers required to introduce a stitch, then the **e**+**f** pathway would be expected to provide product **4** selectively. Fully protected, resin-bound substrate **1** was subjected to RCM under the same conditions as used in the single-RCM reactions described above. LC/MS analysis of the crude reaction mixture revealed 84% conversion to bis-RCM products following three 2-h metathesis reactions (Table 1, entry **XII**). A single major product accounted for ~80% of the total product distribution having the correct molecular mass. A number of minor products having the correct molecular mass and together comprising ~20% of the total product distribution were also observed, but none was formed in sufficient amounts to warrant further characterization. As stapling studies have demonstrated that small amounts of minor double bond isomers (*trans* for i,i+4 and *cis* for *i,i*+7) are formed during peptide stapling RCM reactions, such isomers of the major product are likely to account for the bulk of the minor products observed.

Based on the results of the single-RCM reactions, **4** is the most likely structure for the major bis-RCM product. To further validate this assignment of the stitched product, we performed a Monte Carlo conformational search and identified all low energy conformations of each linker in the helical state. The molecular modeling study indicates that the most stable olefin isomer of **4** is thermodynamically more stable than that of **3** by ~15 kcal/mol. This is in part due to three *syn*-pentane interactions that arise only in product **3**: two involve the spiro junction while the other involves the N-terminal attachment of the *i,i*+4 staple (Figure 2C). Regarding olefin geometry in product **4**, we observed a preference of ~2.5 kcal/mol for a *cis* double bond in the *i,i*+4 staple. Though there is no significant energetic preference for either double bond orientation in the *i,i*+7 staple, the absence of any significant ring constraint most likely results in a *trans* double bond that reflects the intrinsic preference of the catalyst. We have thus far been unable to confirm these predictions by NMR, as the signals for the olefinic protons overlap and show uninterpretable coupling patterns.

Encouraged by the efficiency of the RCM leading to the *i* + 4 + 7 stitched product **4**, we explored the possibility of forming stitched peptides having other stitching configurations. Toward this end, various peptide substrates bearing the olefin-containing amino acid residues at different positions were designed based on the established half-site rules (Table 1, entries **XIII-XVII**). All of the peptide substrates designed to incorporate a stitch composed of two favorable half-site staples underwent a smooth RCM reaction to give the corresponding double-RCM products. It should be noted that the peptide bearing $S_5$ at both positions i and i+8 along with $B_5$ at i+4 (entry **XV**) demonstrated only modest conversion to a complex mixture of four stitched products, with no single major product detected. This particular peptide was designed to further demonstrate the stereoselectivity of RCM reactions on an α-helix scaffold; according to computational and experimental single-RCM studies, the RCM of the pro-(*R*) side-chain of $B_5$ with any of three olefin partners in this substrate would be unfavorable (entries **I**, **III**, and **X**). On the contrary, the pro-(*S*) side-chain of $B_5$ would favorably react with $S_5$ at either position i or i + 8 to form an $S_{i,i+4}S(8)$ staple. The examples provided in entries **XIII-XV** clearly demonstrate that the RCM reactions

**Table 1. Sequences of Peptide Substrates and Percent Conversions for Metathesis Reaction**

| Entry | Sequence | Model | Connectivity | Product | % Conversion[a] | Product Ratio[b] | % Helicity[c] |
|---|---|---|---|---|---|---|---|
| I | EWAETAA$B_5$KFLAAHA | a | | | 23% | | |
| II | EWA$S_5$TAAAKFLAAH$S_8$ | b | i,i+11 | | 0%[d] | | |
| III | EWA$S_5$TAA$R_5$KFLAAHA | c | i,i+4 | | 0%[d] | | |
| IV | EWAETAA$S_5$KFLAAH$S_8$ | d | i,i+7 | | 90% | 1:1 | |
| V | EWA$S_5$TAA$S_5$KFLAAHA | e | i,i+4 | | >95% | 14:1 | |
| VI | EWAETAA$R_5$KFLAAH$S_8$ | f | i,i+7 | | 90% | 3:1 | |
| VII | EWAETAA$R_5$KFL$R_5$AHA | g | i,i+4 | | 95% | 4:1 | |
| VIII | EWA$R_5$TAA$R_5$KFLAAHA | h | i,i+4 | | 94% | 6:1 | |
| IX | EWAETAA$S_5$KFL$S_5$AHA | i | i,i+4 | | 93% | 5:1 | |
| X | EWA$R_5$TAA$S_5$KFLAAHA | j | i,i+4 | | 43% | 2:1 | |
| XI | $R_8$WAETAA$S_5$KFLAAHA | k | i,i+7 | | 82% | 2:1 | |
| XII | EWA$S_5$TAA$B_5$KFLAAH$S_8$ | | i,i+4+7 | 4 | 84% | 4:1 | 86% |
| XIII | EWA$S_5$TAA$B_5$KFL$R_5$AHA | | i,i+4+4 | 5 | >95% | 8:1 | 82% |
| XIV | EWA$R_5$TAA$B_5$KFL$S_5$AHA | | i,i+4+4 | 6 | >95% | 3:1 | 65% |
| XV | EWA$S_5$TAA$B_5$KFL$S_5$AHA | | i,i+4+4 | | 63% | 1:3 | N.D.[e] |
| XVI | $R_8$WAETAA$B_5$KFL$R_5$AHA | | i,i+7+4 | 7 | 63% | 3:2 | 45%/28%[f] |
| XVII | $R_8$WAETAA$B_5$KFLAAH$S_8$ | | i,i+7+7 | 8 | 54% | 1:1 | 69%[g] |
| XVIII | EWAETAAAKFLAAHA | | | 9 | | | 24% |
| XIX | EWAUTAA$R_5$KFLAAH$S_8$[h] | | i,i+7 | 10 | >95% | 4:1 | 60% |
| XX | EWSUTDNUKQEADRU[h] | | | 11 | | | 20% |
| XXI | EWSUTDN$R_5$KQEADR$S_8$[h] | | i,i+7 | 12 | 93% | 1:1 | 36% |
| XXII | EWS$S_5$TDN$B_5$KQEADR$S_8$ | | i,i+4+7 | 13 | >95% | 4:5[i] | 60% |
| XXIII | RRRRRRRRRRRR | | | R12 | | | |
| XXIV | RRRR$R_5$RRRRRR$S_8$ | | i,i+7 | R12-Stp | 84% | N.A.[j] | 23% |
| XXV | $S_5$RRR$B_5$RRRRRR$S_8$ | | i,i+4+7 | R12-Stc | 72% | 1:1 | 59% |
| XXVI | $S_5$RRR$B_5$RRRRRR$S_8$ | | unmetathesized | R12-Unstc | | | 15% |

[a]Percent conversion [desired RCM products/(desired RCM products + intermediates + starting material)] to stitched or stapled products after three 2 h RCM reactions (unless otherwise noted) as determined by reversed-phase HPLC. [b]Ratio of the major stitched (or stapled) final product to the sum of all minor stitched (or stapled) final products as determined by reverse-phase HPLC. [c]Percent helicity was calculated from mean-residue ellipticity at 222 nm ($[\theta]222$) using $-31{,}500(1 - 2.5/n)$ and 0 deg cm$^2$ dmol$^{-1}$ as the values for 100 and 0% helicity, respectively; $n$ is the number of amino acid residues in the peptide.[42] [d]No product detected after two 2 h RCM reactions. [e]Four stitched products were detected with relative abundances of 3:3:2:1. CD studies were not conducted due to the complexity of the reaction. [f]Percent helicity of two major stitched products after isolation. [g]Percent helicity of mixture of four stitched products. [h]U represents $\alpha$-aminoisobutyric acid (Aib), which mimics the helix-stabilizing effect of the $\alpha,\alpha$-disubstituted $S_5$. [i]Four stitched products were detected with relative abundances of 4:2:2:1 [j]A single stapled product was detected.

among multiple olefin side-chains in $\alpha$-helical templates proceed in a highly stereoselective manner.

With a series of stitched peptides in hand, we next investigated the effects of stitching on the conformational preference and structural stability of the peptides. In far ultraviolet CD analyses, the stitched peptides displayed CD spectra characteristic of a typical right-handed $\alpha$-helix (Figure 3A), with a maximum near 195 nm and minima at 208 and 222 nm.[42] Based on the mean residue ellipticity at 222 nm, all of the stitched analogs displayed enhanced $\alpha$-helical character compared to the unmodified parent sequence 9 (Table 1). The $i + 4 + 7$ stitched peptide 4 displays the highest helical content of all the peptides studied here, 86%, which is far higher than that of its $i, i + 7$ single-stapled counterpart 10 (60%) (Figure 3B). Notably, the CD spectrum of 4 is not concentration dependent, suggesting that aggregation is not responsible for the high $\alpha$-helicity of this stitched peptide (Figure S2A). The lower helical content of the $i + 7 + 4$ stitched peptide 7 (45/28%) when compared to 10 (60%) or 4 (86%) may result from a *syn*-pentane interaction that occurs between the two staples of 7. The $\alpha$-helical structure of the stitched peptides was further confirmed by an NMR spectroscopy study of an $i + 4 + 7$ stitched analog 13 possessing enhanced water-solubility (Table 1, entry XXII and Figures

S2B and S2C) using a combination of 2D NOESY and TOCSY spectra (Figures S3 and S4).

To examine the effect of stitching on conformational stability, we compared stitched peptide 4 with its stapled and unmodified counterparts in terms of resistance to thermal and chemical denaturation. In thermal unfolding experiments, stapled peptide 10 underwent a cooperative melting transition with an approximate $T_m$ of 55 °C, which is far higher than that of unmodified peptide 9 ($T_m = 19$ °C) (Figure 3C). Remarkably, the $i + 4 + 7$ stitched peptide 4 showed additional thermal stability, as it retained more than 60% of its $\alpha$-helicity even at 90 °C. However, 4 did not have a cooperative melting transition point in this temperature range, precluding a $T_m$ determination by this method. In an unfolding experiment using guanidinium hydrochloride (GnHCl), 4 resists conformational disruption in response to increasing guanidinium salt up to 6 M, whereas 10 showed a cooperative denaturing behavior reaching a saturation point at ~4 M GnHCl (Figure 3D).

One of the most significant features of stapled peptides is their enhanced cellular uptake by endocytic vesicle trafficking. To test whether stitched peptides retain this important property, we performed fluorescence-activated cell sorting (FACS) analyses on Jurkat cells exposed to the peptides at 37 °C. As expected, both fluorescein-labeled 4 and 10 caused
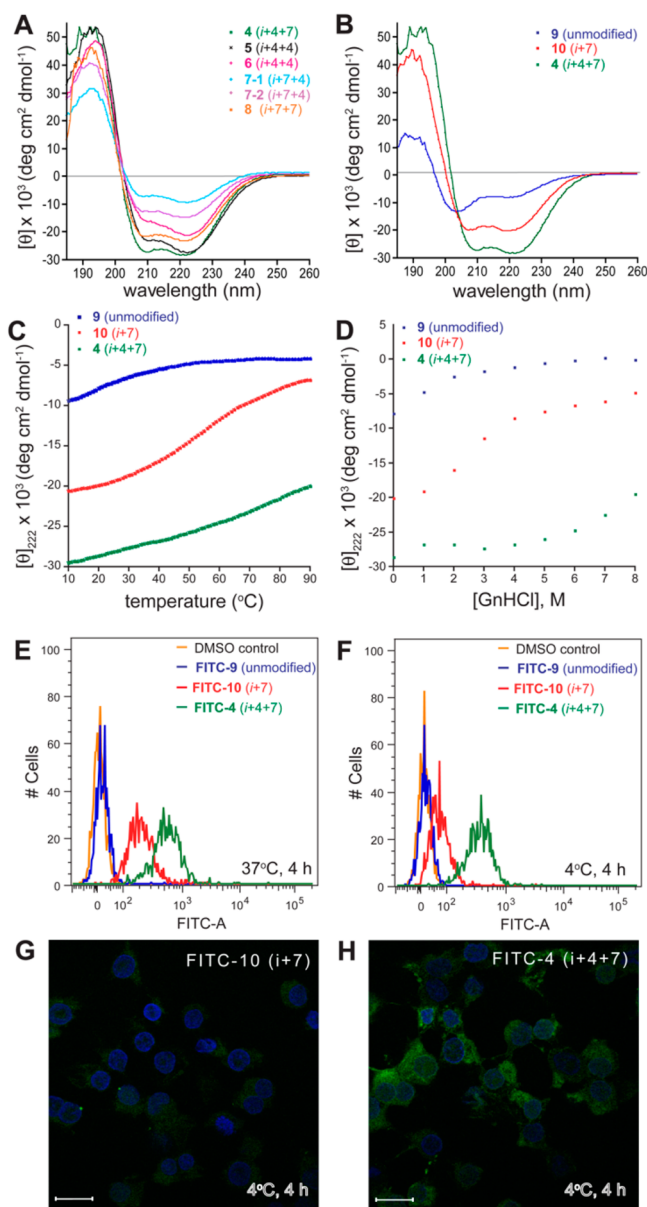
**Figure 3.** (A) CD spectra of stitched peptides at 20 °C. (B) CD spectra of stitched peptide **4** (green) with its unmodified (blue) and stapled (red) counterparts. (C and D) Conformational stability of stitched peptide **4** against thermal (C) and guanidinium hydrochloride denaturation (D) in comparison with its unmodified (blue) and stapled (red) counterparts. Curves were not normalized to demonstrate the different values of each peptide at the highest temperature or guanidinium salt concentration. (E and F) Flow cytometry profile of Jurkat cells treated with stitched peptide **4** in comparison to its unmodified (blue) and stapled (red) analogs at 37 °C (E) and 4 °C (F). (G and H) Confocal microscope images of U2OS cells treated at 4 °C with 2 μM of fluorescein (green)-labeled **10** (G) or **4** (H). The nuclei are stained by 4′6′-diamino-2-phenylindole (DAPI, blue). Scale bars, 20 μm.

an increase in cell fluorescence, indicative of cellular uptake, whereas the unmodified analog **9** did not show any detectable cell permeability (Figure 3E).

Indeed, stitched peptide **4** displayed a higher degree of cell permeability than its stapled counterpart **10**, as evidenced by an increase in mean and median cellular FITC signals. When the experiment was performed at 4 °C, the cellular fluorescence

observed upon treatment with the stapled analog **10** was significantly decreased in comparison to that observed at 37 °C (Figure 3F), which was expected from previous studies.[33,34] Interestingly, however, the cellular uptake of the stitched analog **4** appears to be much less affected by a low temperature than its stapled counterpart as confirmed by FACS (Figure 3F) as well as confocal microscopy (Figure 3G,H). These results imply that passive membrane diffusion may contribute to the cellular uptake of the stitched peptide.

Importantly, it is unclear from the current data whether the observed increase in cell penetration afforded by all-hydro-carbon stitches relative to all-hydrocarbon staples is due to increased helicity, greater hydrocarbon content in the cross-link, or a combination of these factors. It is possible that the difference in cell penetration is the result of a change in the dominant mechanism of cell entry, and future studies will be performed to further investigate the reasons for these observations.

Encouraged by the markedly enhanced cell penetration of stitched peptide **4**, we investigated the effect of stitching on the cell penetration of oligoarginine, a prototypical cell penetrating peptide (CPP).[51,52] Oligoarginines are intrinsically unstructured in solution, mainly due to charge repulsion among the positively charged side-chain guanidinium groups. Therefore, they represent one of the most challenging cases for stabilization in an $\alpha$-helical structure. In addition, oligoarginines are among the most potent CPPs and have been frequently used as cargo-delivery vectors, as reviewed by Brock[51] and Copolovici and colleagues.[52] Limiting the use of oligo-L-arginines in *in vivo* applications, however, is their high susceptibility to enzymatic degradation. We were therefore interested to determine the extent to which stitching could improve the proteolytic stability of oligoarginine.

We prepared an oligo-L-arginine 12-mer (**R12**), one of the most potent oligoarginine CPPs known,[53] along with its *i*, *i* + 7 stapled (**R12-Stp**), *i* + 4 + 7 stitched (**R12-Stc**), and *i* + 4 + 7 unstitched (**R12-Unstc**) analogs (Table 1, entries XXIII–XXVI). CD analyses indicated that unmodified **R12** was essentially devoid of secondary structure. Introduction of a staple improved the helicity to 23% at room temperature (**R12-Stp**), and stitching provided a significant additional increase to 59% (**R12-Stc**) (Figure 4A). On the contrary, **R12-Unstc** displayed only 15% helicity, indicating that global rigidification by macrocyclization plays a more profound role in helix-stabilization than the localized conformational restriction imparted by the introduction of $\alpha,\alpha$-disubstituted amino acids (data not shown).

To further investigate the effect of stitching on the structural dynamics of an oligo-L-arginine 12-mer, we performed fully atomistic molecular dynamics (MD) simulations with explicit water. Whereas the unmodified **R12** exhibits no significant secondary structure during the simulations, the computed helicities for **R12-Stp** and **R12-Stc** are 21.3 and 56.4%, respectively, in excellent agreement with our experimental data (Figures 4B–D). Based on residue-specific helicity calculations, **R12-Stc** displays helical character throughout the entire peptide, whereas the helicity of **R12-Stp** is localized to residues 5–8.

To further understand the molecular origin for the enhanced helix nucleation of all-hydrocarbon-stitching compared to stapling, we performed a solvation analysis to calculate the number of water molecules around each residue of **R12**, **R12-Stp**, and **R12-Stc** in their equilibrium structures. The average

12319

dx.doi.org/10.1021/ja505141j | *J. Am. Chem. Soc.* 2014, 136, 12314−12322
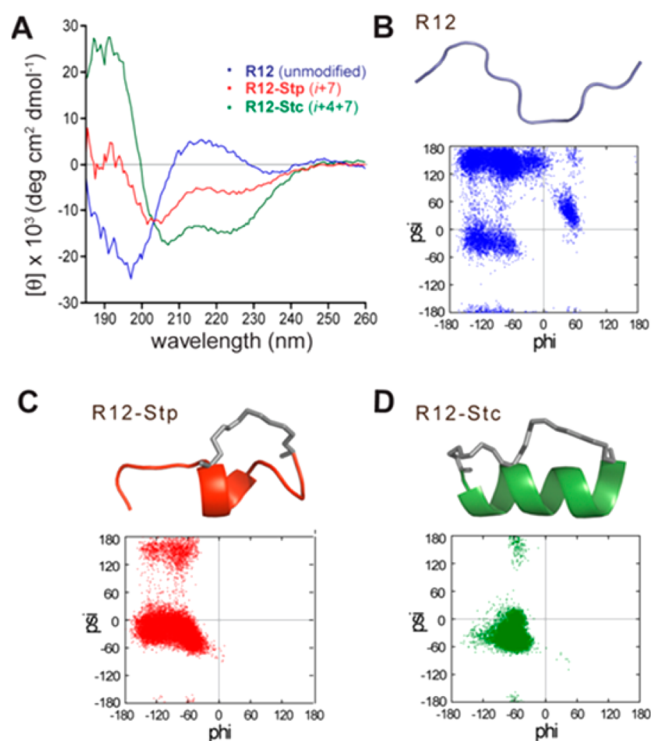
**Figure 4.** (A) CD spectra of dodeca-L-arginine (**R12**) and its stapled (**R12-Stp**) and stitched (**R12-Stc**) analogs at 20 °C. (B−D) The most distributed conformations and the Ramachandran plots of the ensemble structures of each analog. **R12** adopts no defined secondary structure, and **R12-Stc** displays a more extended $\alpha$-helical region than **R12-Stp**.



**Figure 5.** (A) Confocal microscope images of HeLa cells treated with 5 $\mu$M fluorescein (green)-labeled analogs at 37 °C for 1 h in the presence of DAPI (blue). Scale bars, 20 $\mu$m. (B) Quantitative comparison of cellular uptake of fluorescein-labeled peptides using epifluorescence. Error bars represent the mean ± standard deviation of two independent experiments. (C) Stability toward trypsin digestion. **R12-Stc** displays a 20-fold longer half-life ($t_{1/2}$) than **R12-Stp**.

number of water molecules for **R12** is 3.4 per residue, and those water molecules are evenly distributed throughout the peptide. For **R12-Stp**, the average number of water molecules is decreased to 2.5 per residue, and we observed a modest localized dehydration of the peptide backbone spanning residues 4−8. **R12-Stc** displays extensive dehydration of the backbone of residues 2−11, with an average of 1.8 water molecules per residue. Because helix unfolding in an aqueous environment is triggered primarily by the access of water to the backbone hydrogen bonds,[49,50,54] these results indicate that the all-hydrocarbon staples and stitches shield the backbone hydrogen bonds from competition by solvent water molecules. Our experimental and computational analyses, therefore, indicate that the enhanced $\alpha$-helix stabilization conferred by all-hydrocarbon stitching is due to improved conformational rigidification as well as the creation of a more extended hydrophobic microenvironment around the backbone hydrogen bonds.[50]

To examine the effect of peptide stitching on cell penetration, we treated HeLa cells with fluorescein-labeled analogs (5 $\mu$M) at 37 °C for 1 h and analyzed their cellular uptake using confocal microscopy, which revealed that **R12-Stc** fully retained the cell penetrating ability of **R12** (Figure 5A). Furthermore, epifluorescence microscopy analysis using a lower concentration (1 $\mu$M) with a longer incubation time (8 h) indicated that the cellular uptake of **R12-Stp** and **R12-Stc** was increased by 21% and 75%, respectively, compared to **R12** (Figure 5B). It is noteworthy that the stitched analog has the smallest net positive charge, indicating that the number of positively charged residues is not the only factor affecting cell penetration of polycationic CPPs. We also considered the

possibility that the higher cytosolic accumulation of **R12-Stc** may be attributable to enhanced metabolic stability provided by the presence of the stitch, which we assessed by examining the ability of stitching to protect against proteolytic degradation. Oligoarginines are extremely vulnerable to trypsin proteolysis, as trypsin predominantly cleaves at the carboxyl side of positively charged amino acids such as lysine and arginine. As expected, after treatment with trypsin for 5 min at 25 °C at an enzyme/substrate ratio of 1/800, the parent oligoarginine **R12** was completely digested. However, under the same conditions, 41% of the stapled version and 94% of the stitched version remained intact. Indeed, greater than 50% of the stitched analog remained intact even after 60 min of trypsin exposure, with a half-life 20-fold longer ($t_{1/2}$ = 64 min) than the corresponding stapled counterpart ($t_{1/2}$ = 3.1 min) (Figure 5C). These results imply that greater helix stability is accompanied by enhanced resistance to digestion by proteases. The additional macrocyclic bridge in the stitched analog most likely physically blocks the access of the protease to the cleavable residues and also prevents the peptide from adopting the extended conformation required for insertion into the enzyme active site.[55]

## ■ CONCLUSIONS

This work demonstrates that ruthenium-mediated RCM reactions on an $\alpha$-helical peptide scaffold can be remarkably selective for chemically equivalent but stereo- and regiochemically distinct olefins. The stitched $\alpha$-helical peptides thus generated feature exceptional thermal stabilities, and they also exhibit dramatically enhanced stability against chemical denaturation and proteolytic digestion. In addition, the stitched peptides show greatly improved cell penetrating ability compared to stapled peptides. Therefore, we believe stitched peptides warrant further investigation as ligands for chemical genetics applications, next-generation therapeutic agents, and tools for macromolecule cargo delivery.

12320

dx.doi.org/10.1021/ja505141j | J. Am. Chem. Soc. 2014, 136, 12314−12322

## ASSOCIATED CONTENT

### S Supporting Information

General information, synthesis of the $B_5$ amino acid, CD data, mass spectrometry data, NMR methods and spectra, discussion of NMR data, discussion of molecular modeling data, and MD methods. This material is available free of charge via the Internet at http://pubs.acs.org.

## AUTHOR INFORMATION

### Corresponding Authors
gregory_verdine@harvard.edu
sihyun@sookmyung.ac.kr

### Present Addresses
‖College of Pharmacy, Dongguk University, 32 Dongguk-Ro, Ilsandong-Gu, Goyang-Si, Gyeonggi-Do 420−820, Korea.
#Cheminformatics, Merck Research Laboratories, Boston, MA 02115, United States.
○Chemical Biology and Proteomics Laboratory, The Salk Institute for Biological Studies, La Jolla, CA 92037, United States.
⊥Center for Human Genetics Research, Massachusetts General Hospital, Boston, MA 02114, United States.
◆Medical Scientist Training Program, Stony Brook University, Stony Brook, NY 11794, United States.

### Author Contributions
∇These authors contributed equally.

### Notes
The authors declare no competing financial interest.

## ACKNOWLEDGMENTS

## REFERENCES

(1) Hopkins, A. L.; Groom, C. R. Nat. Rev. Drug Discovery 2002, 1, 727.
(2) Guharoy, M.; Chakrabarti, P. Bioinformatics 2007, 23, 1909.
(3) Jochim, A. L.; Arora, P. S. Mol. BioSyst. 2009, 5, 924.
(4) Jochim, A. L.; Arora, P. S. ACS Chem. Biol. 2010, 5, 919.
(5) Osapay, G.; Taylor, J. W. J. Am. Chem. Soc. 1990, 112, 6046.
(6) Yu, C. X.; Taylor, J. W. Tetrahedron Lett. 1996, 37, 1731.
(7) Phelan, J. C.; Skelton, N. J.; Braisted, A. C.; McDowell, R. S. J. Am. Chem. Soc. 1997, 119, 455.
(8) Taylor, J. W. Biopolymers 2002, 66, 49.
(9) Pease, J. H. B.; Storrs, R. W.; Wemmer, D. E. Proc. Natl. Acad. Sci. U.S.A. 1990, 87, 5643.
(10) Jackson, D. Y.; King, D. S.; Chmielewski, J.; Singh, S.; Schultz, P. G. J. Am. Chem. Soc. 1991, 113, 9391.
(11) Leduc, A. M.; Trent, J. O.; Wittliff, J. L.; Bramlett, K. S.; Briggs, S. L.; Chirgadze, N. Y.; Wang, Y.; Burris, T. P.; Spatola, A. F. Proc. Natl. Acad. Sci. U.S.A. 2003, 100, 11273.
(12) Galande, A. K.; Bramlett, K. S.; Burris, T. P.; Wittliff, J. L.; Spatola, A. F. J. Pept. Res. 2004, 63, 297.
(13) Kumita, J. R.; Smart, O. S.; Woolley, G. A. Proc. Natl. Acad. Sci. U.S.A. 2000, 97, 3803.
(14) Cabezas, E.; Satterthwait, A. C. J. Am. Chem. Soc. 1999, 121, 3862.
(15) Cantel, S.; Isaad, A. L. C.; Scrima, M.; Levy, J. J.; DiMarchi, R. D.; Rovero, P.; Halperin, J. A.; D'Ursi, A. M.; Papini, A. M.; Chorev, M. J. Org. Chem. 2008, 73, 5663.
(16) Muppidi, A.; Doi, K.; Edwardraja, S.; Drake, E. J.; Gulick, A. M.; Wang, H. G.; Lin, Q. J. Am. Chem. Soc. 2012, 134, 14734.
(17) Lau, Y. H.; de Andrade, P.; Quah, S.-T.; Rossmann, M.; Laraia, L.; Sköld, N.; Sum, T. J.; Rowling, P. J. E.; Joseph, T. L.; Verma, C.; Hyvönen, M.; Itzhaki, L. S.; Venkitaraman, A. R.; Brown, C. J.; Lane, D. P.; Spring, D. R. Chem. Sci. 2014, 5, 1804.
(18) Frost, J. R.; Vitali, F.; Jacob, N. T.; Brown, M. D.; Fasan, R. ChemBioChem 2013, 14, 147.
(19) Haney, C. M.; Horne, W. S. J. Pept. Res. 2014, 20, 108.
(20) Zou, Y.; Spokoyny, A. M.; Zhang, C.; Simon, M. D.; Yu, H.; Lin, Y. S.; Pentelute, B. L. Org. Biomol. Chem. 2014, 12, 566.
(21) Mazzier, D.; Peggion, C.; Toniolo, C.; Moretto, A. Biopolymers 2014, 102, 115.
(22) Blackwell, H. E.; Grubbs, R. H. Angew. Chem., Int. Ed. 1998, 37, 3281.
(23) Blackwell, H. E.; Sadowsky, J. D.; Howard, R. J.; Sampson, J. N.; Chao, J. A.; Steinmetz, W. E.; O'Leary, D. J.; Grubbs, R. H. J. Org. Chem. 2001, 66, 5291.
(24) Boal, A. K.; Guryanov, I.; Moretto, A.; Crisma, M.; Lanni, E. L.; Toniolo, C.; Grubbs, R. H.; O'Leary, D. J. J. Am. Chem. Soc. 2007, 129, 6986.
(25) Chapman, R. N.; Dimartino, G.; Arora, P. S. J. Am. Chem. Soc. 2004, 126, 12252.
(26) Schafmeister, C. E.; Po, J.; Verdine, G. L. J. Am. Chem. Soc. 2000, 122, 5891.
(27) Kim, Y. W.; Verdine, G. L. Bioorg. Med. Chem. Lett. 2009, 19, 2533.
(28) Kim, Y. W.; Kutchukian, P. S.; Verdine, G. L. Org. Lett. 2010, 12, 3046.
(29) Shim, S. Y.; Kim, Y. W.; Verdine, G. L. Chem. Biol. Drug Des. 2013, 82, 635.
(30) Verdine, G. L.; Hilinski, G. J. Methods Enzymol. 2012, 503, 3.
(31) Verdine, G. L.; Hilinski, G. J. Drug Discovery Today: Technol. 2012, 9, e41.
(32) Walensky, L. D.; Bird, G. H. J. Med. Chem. [Online early access]. DOI: 10.1021/jm4011675 (accessed March 6, 2014).
(33) Walensky, L. D.; Kung, A. L.; Escher, I.; Malia, T. J.; Barbuto, S.; Wright, R. D.; Wagner, G.; Verdine, G. L.; Korsmeyer, S. J. Science 2004, 305, 1466.
(34) Bernal, F.; Tyler, A. F.; Korsmeyer, S. J.; Walensky, L. D.; Verdine, G. L. J. Am. Chem. Soc. 2007, 129, 2456.
(35) Moellering, R. E.; Cornejo, M.; Davis, T. N.; Del Bianco, C.; Aster, J. C.; Blacklow, S. C.; Kung, A. L.; Gilliland, D. G.; Verdine, G. L.; Bradner, J. E. Nature 2009, 462, 182.
(36) Grossmann, T. N.; Yeh, J. T. H.; Bowman, B. R.; Chu, Q.; Moellering, R. E.; Verdine, G. L. Proc. Natl. Acad. Sci. U.S.A. 2012, 109, 17942.
(37) Bird, G. H.; Madani, N.; Perry, A. F.; Princiotto, A. M.; Supko, J. G.; He, X.; Gavathiotis, E.; Sodroski, J. G.; Walensky, L. D. Proc. Natl. Acad. Sci. U.S.A. 2010, 107, 14093.
(38) Chang, Y. S.; Graves, B.; Guerlavais, V.; Tovar, C.; Packman, K.; To, K. H.; Olson, K. A.; Kesavan, K.; Gangurde, P.; Mukherjee, A.; Baker, T.; Darlak, K.; Elkin, C.; Filipovic, Z.; Qureshi, F. Z.; Cai, H.; Berry, P.; Feyfant, E.; Shi, X. E.; Horstick, J.; Annis, D. A.; Manning, A. M.; Fotouhi, N.; Nash, H.; Vassilev, L. T.; Sawyer, T. K. Proc. Natl. Acad. Sci. U.S.A. 2013, 110, E3445.
(39) Green, B. R.; Klein, B. D.; Lee, H. K.; Smith, M. D.; Steve White, H.; Bulaj, G. Bioorganic & medicinal chemistry 2013, 21, 303.
(40) Hao, Y. J.; Wang, C.; Cao, B.; Hirsch, B. M.; Song, J.; Markowitz, S. D.; Ewing, R. M.; Sedwick, D.; Liu, L. L.; Zheng, W. P.; Wang, Z. H. Cancer Cell 2013, 23, 583.
(41) Bird, G. H.; Boyapalle, S.; Wong, T.; Opoku-Nsiah, K.; Bedi, R.; Crannell, W. C.; Perry, A. F.; Nguyen, H.; Sampayo, V.; Devareddy,

A.; Mohapatra, S.; Mohapatra, S. S.; Walensky, L. D. *J. Clin. Invest.* **2014**, *124*, 2113.

(42) Chen, Y. H.; Yang, J. T.; Martinez, H. M. *Biochemistry* **1972**, *11*, 4120.

(43) Favrin, G.; Irback, A.; Samuelsson, B.; Wallin, S. *Biophys. J.* **2003**, *85*, 1457.

(44) *MacroModel*, 9.1 ed.; Schrodinger LLC: New York, NY, 2005.

(45) Still, W. C.; Tempczyk, A.; Hawley, R. C.; Hendrickson, T. *J. Am. Chem. Soc.* **1990**, *112*, 6127.

(46) Clarke, P. A.; Grist, M.; Ebden, M.; Wilson, C.; Blake, A. J. *Tetrahedron* **2005**, *61*, 353.

(47) Clark, J. S.; Marlin, F.; Nay, B.; Wilson, C. *Org. Lett.* **2003**, *5*, 89.

(48) Toniolo, C.; Crisma, M.; Formaggio, F.; Peggion, C. *Biopolymers* **2001**, *60*, 396.

(49) Vila, J. A.; Ripoll, D. R.; Scheraga, H. A. *Proc. Natl. Acad. Sci. U.S.A.* **2000**, *97*, 13075.

(50) Gao, J. M.; Bosco, D. A.; Powers, E. T.; Kelly, J. W. *Nat. Struct. Mol. Biol.* **2009**, *16*, 684.

(51) Brock, R. *Bioconjugate Chem.* **2014**, *25*, 863.

(52) Copolovici, D. M.; Langel, K.; Eriste, E.; Langel, U. *ACS Nano* **2014**, *8*, 1972.

(53) Kosuge, M.; Takeuchi, T.; Nakase, I.; Jones, A. T.; Futaki, S. *Bioconjugate Chem.* **2008**, *19*, 656.

(54) Avbelj, F.; Luo, P.; Baldwin, R. L. *Proc. Natl. Acad. Sci. U.S.A.* **2000**, *97*, 10786.

(55) Tyndall, J. D.; Nall, T.; Fairlie, D. P. *Chem. Rev.* **2005**, *105*, 973.

12322

dx.doi.org/10.1021/ja505141j | *J. Am. Chem. Soc.* 2014, 136, 12314−12322